IOP Publishing Nanotechnology
Nanotechnology 25 (2014) 455301 (8pp) doi:10.1088/0957-4484/25/45/455301

Nanofluidic channels of arbitrary shapes fabricated by tip-based nanofabrication

Huan Hu[1], Yue Zhuo[3], Muhammed E Oruc[4], Brian T Cunningham[1,3] and William P King[1,2]

[1] Department of Electrical and Computer Engineering, University of Illinois at Urbana-Champaign, Urbana, IL-61801, USA
[2] Department of Mechanical Science and Engineering, University of Illinois at Urbana-Champaign, Urbana, IL-61801, USA
[3] Department of Bioengineering, University of Illinois at Urbana-Champaign, Urbana, IL-61801, USA
[4] Department of Chemical and Biomolecular Engineering, University of Illinois at Urbana-Champaign, Urbana, IL-61801, USA

E-mail: wpk@illinois.edu

Received 26 May 2014, revised 17 September 2014
Accepted for publication 23 September 2014
Published 20 October 2014

Abstract

Nanofluidic channels have promising applications in biomolecule manipulation and sensing. While several different methods of fabrication have been demonstrated for nanofluidic channels, a rapid, low-cost fabrication method that can fabricate arbitrary shapes of nanofluidic channels is still in demand. Here, we report a tip-based nanofabrication (TBN) method for fabricating nanofluidic channels using a heated atomic force microscopy (AFM) tip. The heated AFM tip deposits polymer nanowires where needed to serve as etch mask to fabricate silicon molds through one step of etching. PDMS nanofluidic channels are easily fabricated through replicate molding using the silicon molds. Various shapes of nanofluidic channels with either straight or curvilinear features are demonstrated. The width of the nanofluidic channels is 500 nm, and is determined by the deposited polymer nanowire width. The height of the channel is 400 nm determined by the silicon etching time. Ion conductance measurement on one single curvy shaped nanofluidic channel exhibits the typical ion conductance saturation phenomenon as the ion concentration decreases. Moreover, fluorescence imaging of fluid flowing through a fabricated nanofluidic channel demonstrates the channel integrity. This TBN process is seamlessly compatible with existing nanofabrication processes and can be used to achieve new types of nanofluidic devices.

Keywords: nanofluidic channel, tip-based nanofabrication, heated atomic force microscope tip, nanofabrication, nanolithography, heated cantilever, polystyrene

1. Introduction

Nanofluidic channels provide nanometer-scale physical confinement to biomolecules, and therefore are capable for manipulation and analysis of DNA [1–5], proteins [6] and single molecules [7, 8]. Nanofluidic channels also exhibit unique ion transport behavior when at least one dimension of the channel is close to the Debye length [9–13]. Conventional fabrication methods for nanofluidic channels only provide one nanometer-scale dimension, which is the height of the channel [14–18]. To achieve nanometer-scale physical confinement on lateral dimension, advanced nanofabrication techniques such as electron beam lithography (EBL) [19] and focused ion beam (FIB) [20] are required. However, EBL and FIB are expensive and are difficult for massive production of nanofluidic channels. Moreover, EBL and FIB are both serial processes and are not easily scalable. Nanoimprint requires a master mold that is usually expensive to prepare and can only replicate the design of the mold [21, 22]. Several novel nanofluidic channel fabrication methods that rely on certain mechanisms such as elastomeric collapse [23] and wrinkling [24]

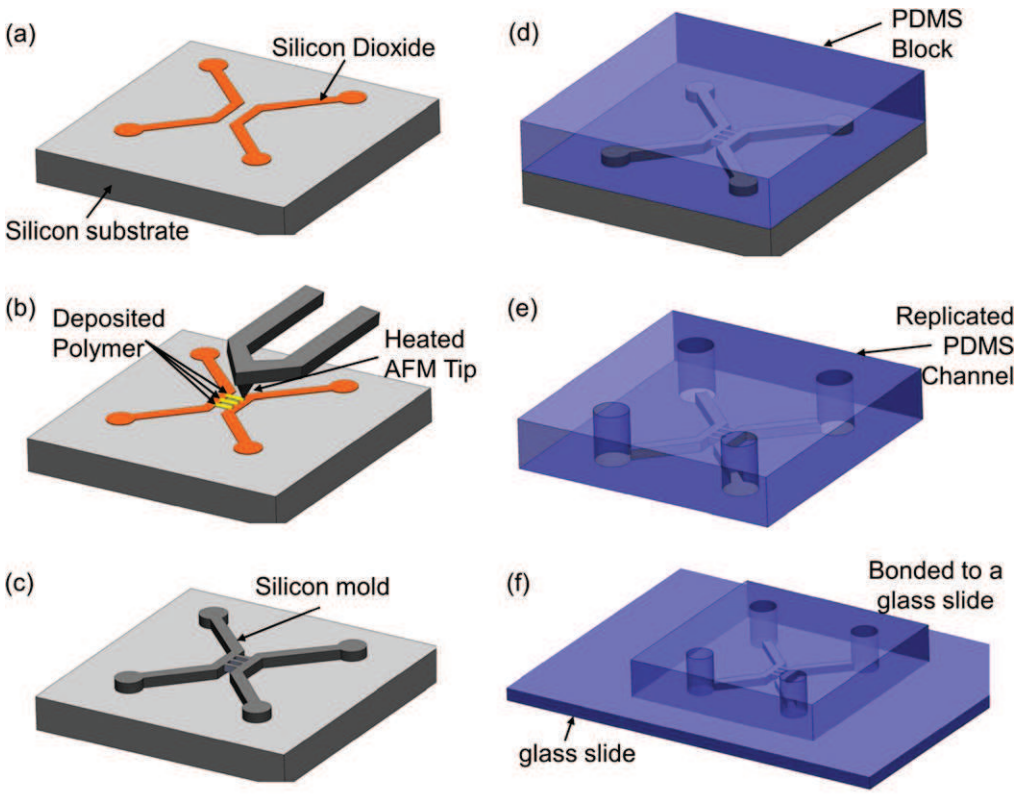

Figure 1. Schematic of major steps in the TBN process for fabricating nanofluidic channels. (a) Fabricate silicon dioxide micropatterns using conventional optical microlithography and wet hydrofluoric acid etching; (b) deposit polymer nanowires across the silicon dioxide micropatterns using a heated AFM tip; (c) Bosch silicon etching using both micropatterned silicon dioxide and polymer nanowires as etch mask; (d) cast PDMS on the fabricated silicon mold; (e) peel off PDMS layer from the silicon mold and punch four through-hole vias as the solution inlets and outlets; (f) bond PDMS channel to a glass slide.

have the advantages of low-cost and simplicity in fabrication, but the design flexibility is relatively limited.

Tip-based nanofabrication (TBN) uses a nanometer scale tip to interact with substrate to define nanoscale features through a number of mechanisms such as manipulation, mechanical scratch, chemical diffusion, thermal indentation, thermal deposition, electrochemical reaction, plasma and etc. TBN employs either scanning tunneling microscopy [25–27] or atomic force microscopy (AFM) [28], either of which cost much lower than EBL and FIB. Moreover, TBN has the potential of achieving parallelization through using array of tips [29, 30]. However, very few publications reported the use of TBN for fabricating nanofluidic channels [31, 32]. One essential reason is that most TBN methods are not compatible with existing nanofabrication method and are difficult to fabricate solid-state materials easily.

This paper presents a TBN method for fabricating arbitrary shapes of nanofluidic channels. We used a heated AFM tip to deposit dense polymer nanowires that served directly as an etch mask to fabricate silicon nanostructures through one step of etching [33]. The silicon nanostructures were used as a mold for replicating PDMS nanofluidic channels. This TBN process is compatible with existing nanofabrication methods.

2. Experiment

Figure 1 shows the major steps in the fabrication process of the nanofluidic channels. The first step (figure 1(a)) was to fabricate micro-patterned silicon dioxide. Starting with a [100] silicon wafer, 70 nm thick silicon dioxide layer was grown in a 1000 °C oxidation furnace for 2 h, followed by patterning photoresist using conventional optical lithography, and then etching the silicon dioxide unprotected by the photoresist using buffered hydrofluoric acid (BHF). The second step (figure 1(b)) was to deposit polystyrene (PS) nanowires using the heated AFM tip.

The PS was loaded onto the tip by bringing the heated AFM tip into contact with a thin PS fiber under a stereo microscope. Upon contact, the heated tip melted the PS, and the PS flowed onto the tip. Upon cooling, the polymer became a solid. The polymer-coated tip was mounted into an Asylum Research MFP-3D AFM, and the tip was scanned along a programmed path with a tip scanning speed of 150 nm s^{-1}. A closed-loop feedback circuit maintained cantilever at a temperature of 260 °C, while the molten PS flowed from the tip to the silicon substrate [34, 35]. After adding the PS polymer, the tip may have too much polymer, and initial nanowires deposited are usually very wide and thick.

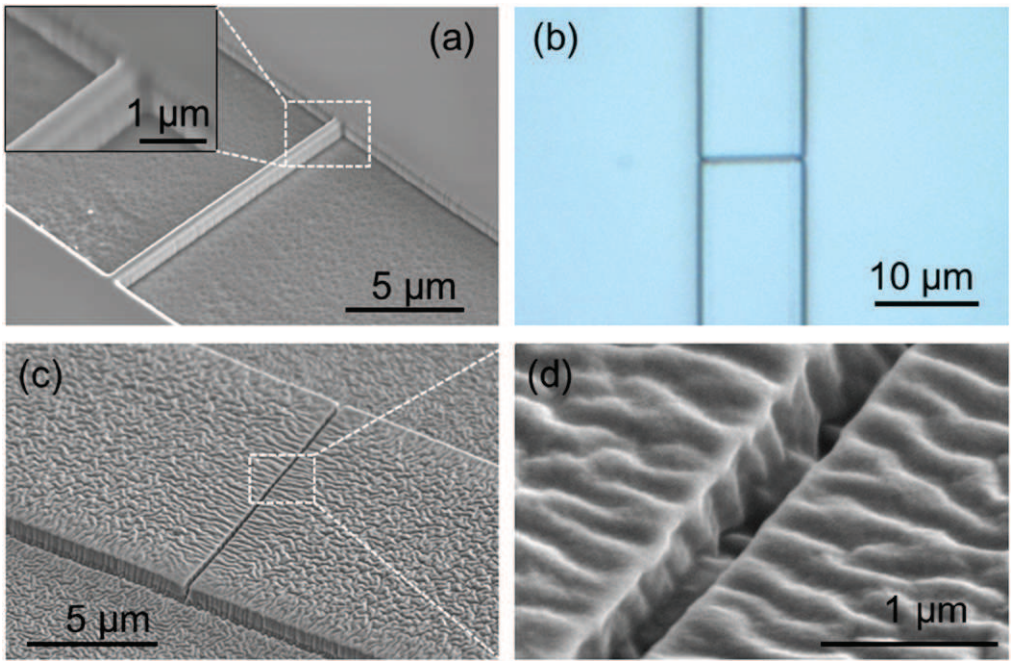

Figure 2. (a) SEM image of a silicon single linear nanochannel mold; the inset image shows the zoomed-in view of a section of the nanochannel mold; (b) a microscopic image of the PDMS nanofluidic channel replicated from the silicon mold as shown above; (c) a SEM image of the PDMS nanofluidic channel replicated; (d) a zoomed-in view of a section of the PDMS nanofluidic channel replicated.

However after several PS nanowire depositions, the width and thickness of the deposited PS becomes stable. The third step (figure 1(c)) was to etch silicon using Bosch process for 1 min with micro-patterned silicon dioxide and deposited PS nanowires. The PS nanowires and the silicon dioxide together served as etch mask [33]. The etching selectivity of PS to silicon is 1 : 80 for this process. To reduce the scallops present on the sidewalls of the silicon structures fabricated by the Bosch process, we tuned the etching step to be 2.5 s and the passivation step to be 1.5 s. After etching, the remaining silicon was used later as a mold for replicating PDMS nanofluidic channels. The fourth step (figure 1(d)) was to mold PDMS with the fabricated silicon mold. We mixed PDMS (sylgard 184) base with a curing agent at a mass ratio of 4 : 1. After degassing the mixture, we poured the mixture on top of the silicon master and heated at 60 °C hotplate for 12 h to cure the PDMS. To facilitate the PDMS demolding, we deposited 15 nm thick amorphous fluorocarbon film on the silicon mold using sputtering before pouring PDMS on the silicon mold [36]. The fifth step (figure 1(e)) was to peel the PDMS channel layer off and manually punch four through-holes on the cured PDMS channel later serving as liquid inlets and outlets. The last step (figure 1(f)) was to bond this PDMS channel to a glass slide. Before bonding, the glass slide surface was cleaned with acetone, isopropyl alcohol (IPA), water, IPA in sequence and finally blown dry. Then the glass slide and the PDMS channels were both treated using 100 W oxygen plasma for 20 s. Finally, the PDMS surface was brought into contact with glass slide surface and baked at 90 °C hotplate for 20 min.

Figure 2 shows the fabrication results for a single nanofluidic channel using the above-described process. Figure 2(a) is a SEM image of a silicon mold and the inset image shows a zoomed-in view of the silicon mold. The silicon mold has a length of 10 μm, a width of 380 nm, a height of 900 nm. Figure 2(b) is a microscopic image of the PDMS nanofluidic channel replicated from the silicon mold shown in figure 2(a). Figure 2(c) shows a SEM image of the nanofluidic channel. To avoid electron charging effect and obtain good SEM images, we coated the PDMS nanofluidic channel with a 2.5 nm thick Gold film by sputtering. The wrinkles shown at the PDMS surface is due to the swelling of PDMS during the sputtering [37, 38]. Figure 2(d) is the zoomed-in view of the PDMS nanofluidic channel. The nanofluidic channel is 10 μm long, 300 nm wide and 500 nm deep.

Figure 3 shows the fabrication results of two different nanofluidic channel arrays using the present TBN process. Figure 3(a) shows a SEM image of the silicon mold used for producing an array of ten linear nanofluidic channels and figure 3(b) shows an optical microscopic image of the corresponding replicated PDMS nanofluidic channel array. Figure 3(c) shows a SEM image of a PDMS nanofluidic channel array, taken in an environmental SEM at a pressure of 1 Torr with water vapor (FEI XL30 ESEM–FEG). Environmental SEM allows imaging of the PDMS nanofluidic channels a without metal coating [39]. Figure 3(d) shows a SEM image of the silicon mold used to fabricate an array of ten curved nanofluidic channels while figure 3(e) shows a microscope image of the corresponding replicated PDMS nanofluidic channel array. Figure 3(f) shows a SEM image of ten curved PDMS nanofluidic channel array using the environmental SEM also at a pressure of 1 Torr with water vapor. The length of the nanofluidic channel is 10 μm, the width is 300 nm and the depth is about 500 nm.

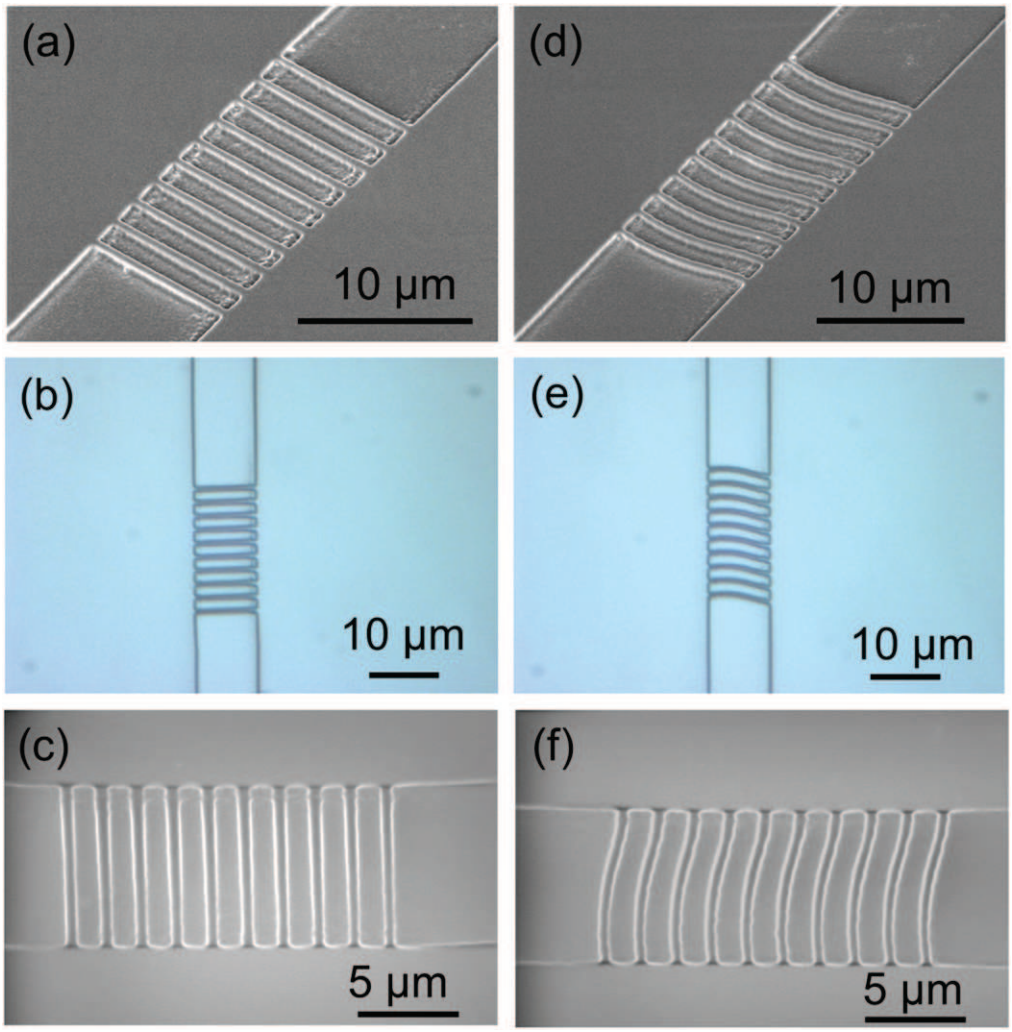

Figure 3. (a) SEM image of the silicon mold used for an array consisting of ten linear nanofluidic channels; (b) microscope image of a replicated PDMS nanofluidic channel array consisting of ten linear nanofluidic channels; (c) environmental SEM image of the PDMS linear nanofluidic channel array replicated using the silicon mold as shown in figure 3(a); (d) SEM image of the silicon mold used for an array consisting of ten curvy nanofluidic channels; (e) microscope image of a replicated PDMS nanofluidic channel array consisting of ten curvy nanofluidic channels; (f) environmental SEM image of the PDMS curvy nanofluidic channel array using the silicon mold shown in figure 3(d).

To show the flexibility of this TBN fabrication process, we fabricated PDMS nanofluidic channel arrays with more complex shapes using the TBN process. Figure 4(a) shows a SEM image of the silicon mold for an array of four wavy-shaped nanofluidic channels while figure 4(b) shows a zoomed-in view of one wavy-shaped silicon mold. The nanofluidic channel width is 250 nm and the channel depth is about 800 nm. Figure 4(c) shows an environmental SEM image of the PDMS nanofluidic channels replicated using the silicon mold as shown in figure 4(a) while figure 4(d) shows a regular SEM image of the same PDMS nanofluidic channel coated with 5 nm thick Au/Pd film. In regular SEM imaging, thin metal films must be coated on the PDMS sample, which induces wrinkles in the PDMS surface, and can also cause channel sealing as shown in figure 4(d). The environmental SEM provides imaging of intact PDMS nanofluidic channels.

3. Results and discussion

In this TBN process, the nanofluidic channel depth is controlled by the silicon mold height, which can be adjusted by changing the etching duration. In turn, the shape of the nanofluidic channels is determined by the PS nanowire geometries. Using the conditions described here, we can deposit PS nanowires with a minimum radius of curvature about 2 μm, however smaller radii could not be reliably fabricated due to the dynamics of polymer flow on the substrate. The nanofluidic channel width is determined by the width of the PS nanowires deposited using the heated AFM tip, which is usually in the range of several hundred nanometers [33]. To reduce the nanofluidic channel width, we thinned down the silicon mold features using silicon thermal oxidation followed by BHF etching. For every unit of silicon oxide that is consumed, 0.46 units of silicon is consumed. A 200 nm thick

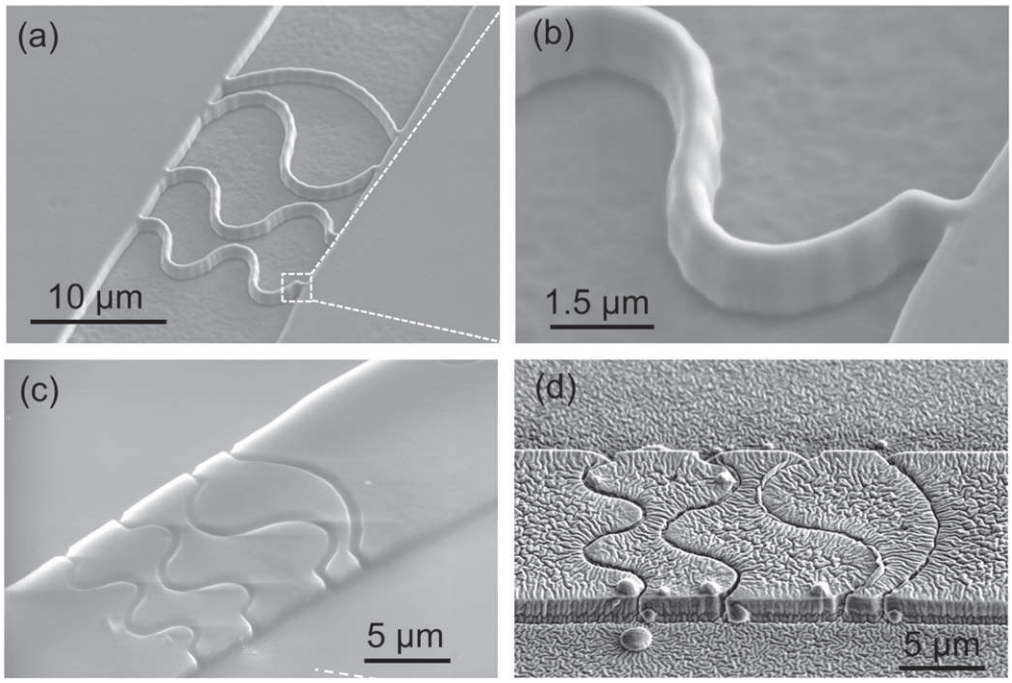

Figure 4. (a) SEM image of the silicon mold for an array of four wavy shapes of the nanofluidic channel with half, one, one and half and two full waves; (b) zoomed-in view of the silicon mold for the wavy shapes of the nanofluidic channel; (c) environmental SEM image of the PDMS nanofluidic channels replicated using the silicon mold as shown in figure 4(a); (d) regular SEM image of the PDMS nanofluidic channels with 5 nm film of Au/Pd for conductive coating.

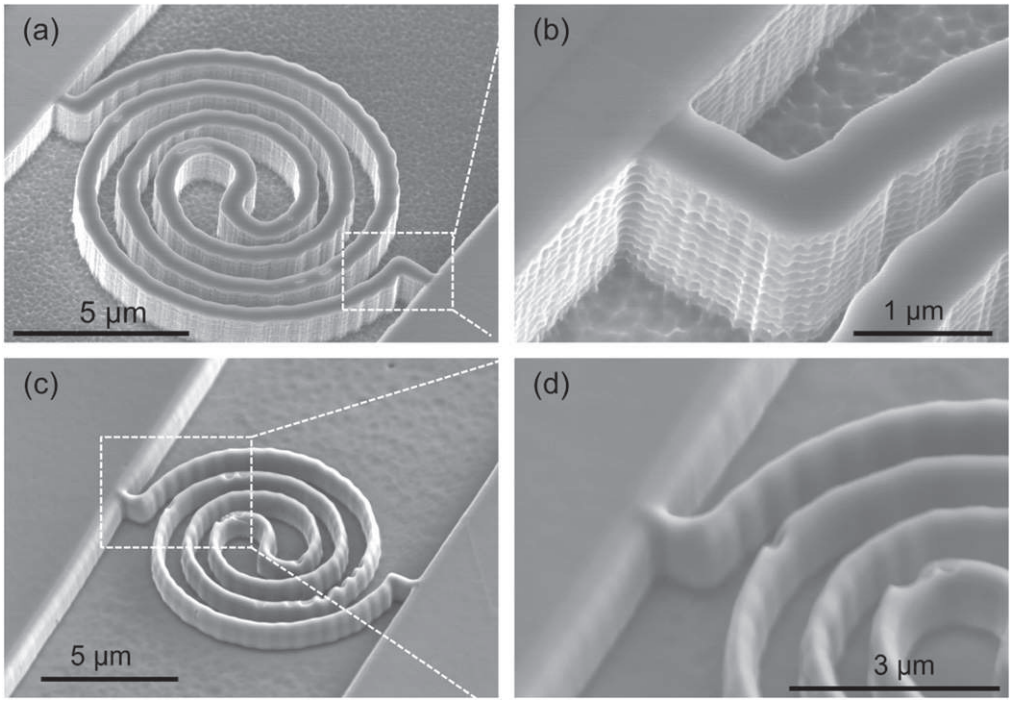

Figure 5. (a) SEM of a spiral-shaped silicon mold that was fabricated using TBN and Bosch Etch; (b) a zoomed-in view of a section of the silicon mold. The scallops are visible on the sidewall of the silicon mold; the width of the silicon mold is about 500 nm; (c) SEM image of the same spiral-shaped silicon mold that is thinned down using 200 nm oxidation and BHF etching; (d) zoomed-in view of a section of the silicon mold. The scallops are removed by the thinning down process. The width of the silicon mold after thinning down reduces to 300 nm.

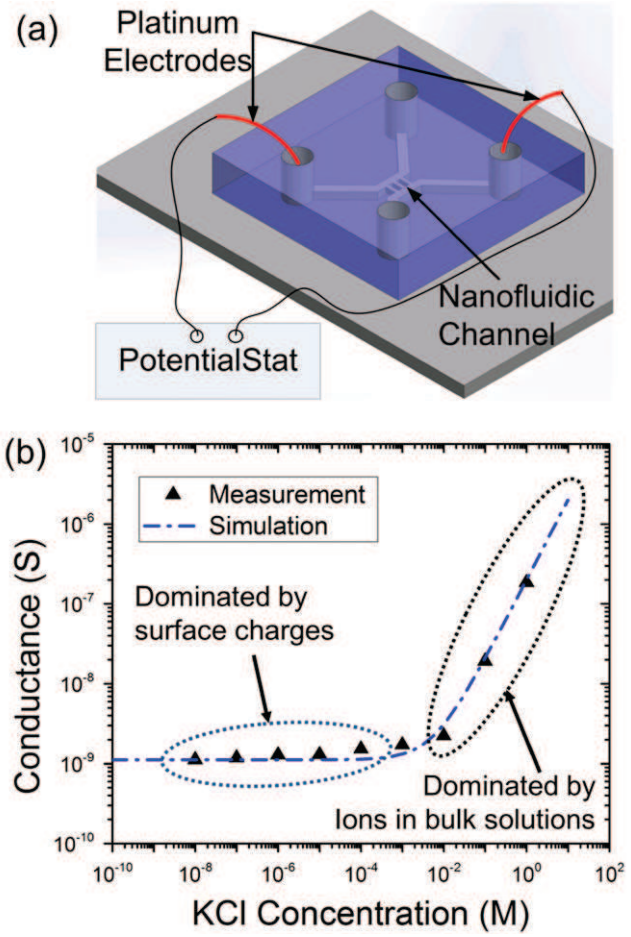

Figure 6. (a) Schematic showing the measurement setup for the current–voltage measurement of PDMS nanofluidic channels; (b) measured and modeled nanofluidic channel conductance at different KCL concentrations.

silicon oxidation process consumes around 92 nm thick silicon. This thinning process also reduces the sidewall roughness of the silicon mold structure. Figure 5 shows the silicon mold structure before and after the thinning down. Figures 5(a) and (b) show the SEM image of the silicon mold after DRIE Etching, the silicon mold has a width about 500 nm and scallops are clearly visible. Figures 5(c) and (d) show the SEM image of the silicon mold after 20 min oxygen plasma treatment, 200 nm thermal oxidation, and BHF etching. The silicon mold width reduced to about 370 nm, and the sidewall surface roughness was significantly reduced.

One important characteristic of the nanofluidic channel is the ion transport behavior, particularly the influence of surface charges on the conductance of the nanofluidic channel [33, 40, 41]. We used a single curvy PDMS nanofluidic channel for the measurement of ion transport. First, potassium chloride (KCl) solutions were filled into channels via a plastic tube inserted on one of the through-hole on the PDMS channel with the use of a syringe pump. This filling process ended when both microfluidic channels and the nanofluidic channel were filled. Then we inserted two platinum wires of 400 μm diameter into two through-holes of 1.5 mm diameter residing on opposite sides of nanofluidic channel for electrical connections. We measured the current at different voltages stepping from −5 V to 5 V with a potentiostat (Gamry potentiostat Reference 600) as shown in figure 6(a). In the experiment, KCl solutions with concentration ranging from 10 nM to 1 M were used for different sets of current–voltage (*I–V*) measurements. By fitting the *I–V* curves, conductances of the nanofluidic channel at different KCl concentrations can be derived. Figure 6(b) shows the derived conductances of the nanofluidic channel at different KCl concentrations represented by the black square dots.

In our experiment, *I–V* measurement started after both microfluidic channels sitting at opposite ends of the nanofluidic channel were filled and fluidic flow through the nanofluidic channel stopped. Therefore, the electric current was mostly contributed by the ion migrations inside the nanofluidic channel. The conductance G of a nanofluidic channel can be simplified as equation (1) as shown below [42],

$$G = q\left(\mu_{\mathrm{k}} + \mu_{\mathrm{Cl}}\right) n_{\mathrm{b}} \frac{WH}{L} + 2\mu_{\mathrm{K}}\sigma_{\mathrm{s}}\frac{W}{L}, \qquad (1)$$

where μ_{k} and μ_{Cl} are the mobility of potassium ion and chloride ion, σ_{s} is the nanofluidic channel surface charge density. W, H, and L are the nanofluidic channel width, height and length, and n_{b} is the ion density of the solutions. The first term in equation (1) is due to bulk ion concentration while the second term is due to ions induced by the channel surface charges. At high ion concentrations, the surface charges in a nanofluidic channel are shielded by the mobile ions and have negligible influence on the ion conductance; therefore, the conductance is determined by the bulk concentration. At low ion concentrations, surface charge governs the ion concentration inside the nanofluidic channel, thus dominates the ion conductance.

Nanofluidic channel used in this *I–V* measurement has a width of 400 nm, a height of 400 nm and a length of 12 μm. To calculate the surface charge density, we chose μ_{k} to be 7.619×10^{-8} m^2 V^{-1} s^{-1} and μ_{Cl} to be 7.912×10^{-8} m^2 V^{-1} s^{-1} [42]. Based on the experiment data, we derived the surface charge density σ_{s} to be 0.22 C m^{-2}, close to the reported values of surface charge density of 0.1 C m^{-2} for silicon dioxide [11, 43]. Figure 6(b) shows the simulation curve based on equation (1) as represented by the solid black dash dot curve. As the KCl concentration reduces from 1 M to 1 mM, the nanofluidic channel conductance decreases proportionally to the KCl concentration. As the KCl concentration keeps on decreasing below 10 μM, the nanofluidic channel conductance stops decreasing proportionally to the KCl concentration and starts to saturate, which is a typical behavior widely observed in nanofluidic channels due to the influence of surface charges on the channel walls [9, 10, 42].

Fluorescence microscopy on the single curved PDMS nanofluidic channel was employed to verify the functionality of the nanofluidic channel. First, nanofluidic channel was manually filled with a fluorescent dye (LD-700, Exciton) that was diluted with deionized water to a concentration of the 0.5 mg mL^{-1} using a syringe. The fluorescence dye has a peak absorption wavelength of 647 nm and a peak emission

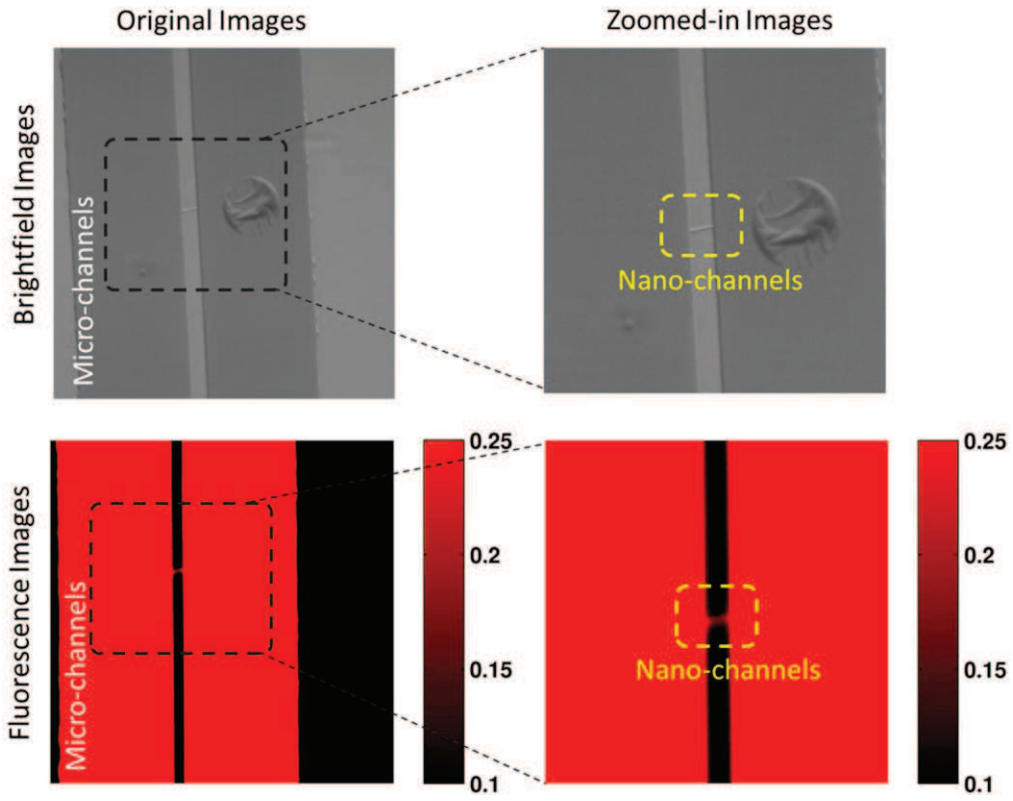

Figure 7. Bright field microscope images and corresponding fluorescence images of a single curved PDMS nanofluidic channel interfacing with two microfluidic channels.

wavelength of 673 nm. Then we used a laser diode with wavelength of 655 nm as the excitation laser and used an inverted microscope (Carl Zeiss Axio Observer Z1) imaging system equipped with a CCD camera (Photometrics Cascade) to capture the fluorescence microscopy images and then plotted the images with a computational software (Matlab, Mathworks). Figures 7(a) and (b) show the bright field microscope images of the nanofluidic channel interfacing two microfluidic channels. Figures 7(c) and (d) are the fluorescence images of the nanofluidic channel showing that the nanofluidic channel was filled with fluorescence dyes, demonstrating the integrity of the nanofluidic channel fabricated by our TBN process.

4. Conclusions

In conclusion, this paper presents the fabrication of PDMS nanofluidic channels using a heated AFM tip. The heated AFM tip deposited PS nanowires on silicon to serve as etch mask to fabricate silicon molds for nanofluidic channels through one step of dry etching. Then PDMS nanofluidic channels were fabricated using the silicon mold through replica molding. We integrated this TBN method with standard nanofabrication process seamlessly to fabricate nanofluidic channel with two interfacing microfluidic channels defined by conventional optical lithography. Both ion conductance measurement and fluorescence imaging were carried out on one of the fabricated nanofluidic channels for demonstrating the functionality. This TBN method of fabricating nanofluidic channels is rapid, low-cost and has the potential of scaling up for massive production of nanofluidic channels. Moreover, this TBN method can create arbitrary shapes of nanofluidic channels and is seamlessly compatible with existing nanofabrication process, which makes this method suitable for producing highly-integrated lab-on-chip nanofluidic devices with complex structures such as a funnel [44].

Acknowledgments

This work was supported by the NSF Center for Nano-Chemical-Electro-Mechanical Manufacturing Systems (Nano-CEMMS) and DARPA. We also would like to thank Yaguang Lian for the help of developing the Bosch process, Scott Robinson and Cate Wallace for the help on using the environmental SEM.

References

[1] Han J and Craighead H G 2000 Separation of long DNA molecules in a microfabricated entropic trap array *Science* **288** 1026–9
[2] Riehn R *et al* 2006 A nanofluidic railroad switch for DNA *Nano Lett.* **6** 1973–6

[3] Han J and Craighead H G 1999 Entropic trapping and sieving of long DNA molecules in a nanofluidic channel *J. Vac. Sci. Technol.* A **17** 2142–7
[4] Guo L J *et al* 2004 Fabrication of size-controllable nanofluidic channels by nanoimprinting and its application for DNA stretching *Nano Lett.* **4** 69–73
[5] Bonthuis D J *et al* 2008 Conformation and dynamics of DNA confined in slitlike nanofluidic channels *Phys. Rev. Lett.* **101** 108303
[6] Wang Y C *et al* 2005 Million-fold preconcentration of proteins and peptides by nanofluidic filter *Anal. Chem.* **77** 4293–9
[7] Cipriany B R *et al* 2010 Single molecule epigenetic analysis in a nanofluidic channel *Anal. Chem.* **82** 2480–7
[8] Reisner W *et al* 2010 Single-molecule denaturation mapping of DNA in nanofluidic channels *Proc. Natl. Acad. Sci. USA* **107** 13294–9
[9] Daiguji H *et al* 2004 Ion transport in nanofluidic channels *Nano Lett.* **4** 137–42
[10] Stein D *et al* 2004 Surface-charge-governed ion transport in nanofluidic channels *Phys. Rev. Lett.* **93** 035901
[11] Karnik R *et al* 2005 Electrostatic control of ions and molecules in nanofluidic transistors *Nano Lett.* **5** 943–8
[12] Vlassiouk I and Siwy Z S 2007 Nanofluidic diode *Nano Lett.* **7** 552–6
[13] Kuo T C *et al* 2003 Gateable nanofluidic interconnects for multilayered microfluidic separation systems *Anal. Chem.* **75** 1861–7
[14] Mao P and Han J Y 2005 Fabrication and characterization of 20 nm planar nanofluidic channels by glass–glass and glass-silicon bonding *Lab Chip* **5** 837–44
[15] Haneveld J *et al* 2003 Wet anisotropic etching for fluidic 1D nanochannels *J. Micromech. Microeng.* **13** S62–6
[16] Sparreboom W *et al* 2008 Rapid sacrificial layer etching for the fabrication of nanochannels with integrated metal electrodes *Lab Chip* **8** 402–7
[17] Eijkel J C T *et al* 2004 1D nanochannels fabricated in polyimide *Lab Chip* **4** 161–3
[18] Han A P *et al* 2006 Design and fabrication of nanofluidic devices by surface micromachining *Nanotechnology* **17** 2498–503
[19] Harnett C K *et al* 2001 Heat-depolymerizable polycarbonates as electron beam patternable sacrificial layers for nanofluidics *J. Vac. Sci. Technol.* B **19** 2842–5
[20] Cannon D M *et al* 2004 Fabrication of single nanofluidic channels in poly(methylmethacrylate) films via focused-ion beam milling for use as molecular gates *Appl. Phys. Lett.* **85** 1241–3
[21] Liang X G *et al* 2007 Single sub-20 nm wide, centimeter-long nanofluidic channel fabricated by novel nanoimprint mold fabrication and direct imprinting *Nano Lett.* **7** 3774–80
[22] Cao H *et al* 2002 Fabrication of 10 nm enclosed nanofluidic channels *Appl. Phys. Lett.* **81** 174–6
[23] Park S M *et al* 2009 A method for nanofluidic device prototyping using elastomeric collapse *Proc. Natl. Acad. Sci. USA* **106** 15549–54
[24] Chung S *et al* 2008 Non-lithographic wrinkle nanochannels for protein preconcentration *Adv. Mater.* **20** 3011–6
[25] Kolb D M *et al* 1997 Nanofabrication of small copper clusters on gold(111) electrodes by a scanning tunneling microscope *Science* **275** 1097–9
[26] Lyo I W and Avouris P 1991 Field-induced nanometer-scale to atomic-scale manipulation of silicon surfaces with the stm *Science* **253** 173–6
[27] Hla S W *et al* 2000 Inducing all steps of a chemical reaction with the scanning tunneling microscope tip: towards single molecule engineering *Phys. Rev. Lett.* **85** 2777–80
[28] Tseng A A 2011 Advancements and challenges in development of atomic force microscopy for nanofabrication *Nano Today* **6** 493–509
[29] Somnath S *et al* 2014 Parallel nanoimaging and nanolithography using a heated microcantilever array *Nanotechnology* **25** 014001
[30] Pires D *et al* 2010 Nanoscale three-dimensional patterning of molecular resists by scanning probes *Science* **328** 732–5
[31] Harfenist S A *et al* 2004 Direct drawing of suspended filamentary micro- and nanostructures from liquid polymers *Nano Lett.* **4** 1931–7
[32] Pellegrino L *et al* 2006 (Fe,Mn)3O4 nanochannels fabricated by AFM local-oxidation nanolithography using Mo/Poly (methyl methacrylate) nanomasks *Adv. Mater.* **18** 3099–104
[33] Huan H *et al* 2013 Fabrication of arbitrarily shaped silicon and silicon oxide nanostructures using tip-based nanofabrication *J. Vac. Sci. Technol.* B **31** 06FJ01
[34] Jonathan R F *et al* 2012 Nanometer-scale flow of molten polyethylene from a heated atomic force microscope tip *Nanotechnology* **23** 215301
[35] Somnath S *et al* 2011 Improved nanotopography sensing via temperature control of a heated atomic force microscope cantilever *IEEE Sensors J.* **11** 2664–70
[36] Huan H *et al* 2012 Nano-fabrication with a flexible array of nano-apertures *Nanotechnology* **23** 175303
[37] Chan E P and Crosby A J 2006 Fabricating microlens arrays by surface wrinkling *Adv. Mater.* **18** 3238–42
[38] Breid D and Crosby A J 2009 Surface wrinkling behavior of finite circular plates *Soft Matter* **5** 425–31
[39] Danilatos G D 1993 Bibliography of environmental scanning electron microscopy *Microsc. Res. Tech.* **25** 529–34
[40] Daiguji H *et al* 2003 Ion transport in nanofluidic channels *Nano Lett.* **4** 137–42
[41] Eijkel J C T and van den Berg A 2005 Nanofluidics: what is it and what can we expect from it? *Microfluid. Nanofluid.* **1** 249–67
[42] Cheng L-J 2008 *Ion and Molecule Transport in Nanochannels* (Ann Arbor: ProQuest)
[43] Stein D *et al* 2004 Surface-charge-governed ion transport in nanofluidic channels *Phys. Rev. Lett.* **93** 035901
[44] Perry J M *et al* 2010 Ion transport in nanofluidic funnels *ACS Nano* **4** 3897–902